Surface & Coatings Technology 203 (2009) 1293–1297

Contents lists available at ScienceDirect

Surface & Coatings Technology

journal homepage: www.elsevier.com/locate/surfcoat

Influence of microstructure on the corrosion behavior of nitrocarburized AISI H13 tool steel obtained by pulsed DC plasma

R.L.O. Basso [a,*], R.J. Candal [b], C.A. Figueroa [a], D. Wisnivesky [a], F. Alvarez [a]

[a] Instituto de Física "Gleb Wataghin", Unicamp, 13083-970 Campinas, São Paulo, Brazil
[b] INQUIMAE-UBA, Ciudad Universitaria, Pabellón II, 1428-Buenos Aires, Argentina

ARTICLE INFO

Article history:
Received 19 February 2008
Accepted in revised form 1 October 2008
Available online 17 October 2008

Keywords:
Plasma nitrocarburizing
Steel corrosion
Tool steel
X-ray diffraction
Surface porosity
Porosity analysis

ABSTRACT

The influence of microstructure on the corrosion behavior of pulsed plasma nitrocarburized AISI H13 tool steel in NaCl 0.9 wt/V % solution is reported. The samples were prepared with different nitrocarburizing treatment times using a constant [CH_4/H_2+N_2] gaseous mixture by a DC pulsed plasma system. The microstructure of the nitrocarburized layers was analyzed by scanning electron microscopy (SEM), X-ray photoelectron spectroscopy (XPS) and X-ray diffraction. The corrosion behavior was evaluated by potentiodynamic polarization experiments. The nitrocarburizing process considerably improves the corrosion resistance of the material in a NaCl environment as compared to the untreated H13 steel. The modified surface layer mainly consisting of ε-Fe_{2-3}(C,N) and γ′-Fe_4N phases confers this outstanding behavior. The corrosion resistance dependence on specific nitrocarburizing processes is reported and the role of the surface porosity is discussed.

1. Introduction

Plasma treatments are techniques commonly used to generating coatings that improves the surface properties of metallic materials, such as wear and corrosion resistance [1–4]. These techniques can introduce large non-equilibrium concentrations of alloying elements into the material by causing chemical, composition, and microstructure changes in the treated layer, providing protective surface modifications when exposed to aggressive environments [5–9]. For example, the introduction of nitrogen in austenitic steels improves its mechanical properties and can strongly affect corrosion resistance. Indeed, depending on the corrosive environment and the preparation process, the corrosion resistance can be augmented or diminished [10]. Some steels, like the AISI H13 tool steel, are commonly used in aggressive environments. The wear resistance of these materials is notably improved by thermo-chemical surface treatment based on nitriding pulsed plasma techniques [11]. It leads to the formation of hard iron carbonitrides due to carbon and nitrogen diffusion occurring on the steel surfaces at temperatures below the eutectoid temperature (~593 °C) [12]. The main phases formed are the ε-Fe_{2-3}(C,N) carbonitride and γ′-Fe_4N nitride, and due to their high hardness values, they increase the strength and life time of steels under friction and wear environments [13–15]. Some studies have demonstrated that the best wear properties are obtained when the surface layer mainly consists of a compact monolayer close-packed hexagonal ε-Fe_{2-3}(N,C) phase [16–19]. This is so because a nitride layer formed by a ε-Fe_{2-3}(C,N) and γ′-Fe_4N mixture is stressed by the mismatching crystalline constituents. Despite the importance of this tool material, to the author's knowledge, the corrosion behavior of nitrocarburized H13 steel is not reported in the specialized literature.

In the present paper, the influence of the microstructure on the corrosion resistance of plasma nitrocarburized H13 steel prepared at several treatment times and conditions is reported. The microstructure of the nitrocarburized layers is analyzed by scanning electron microscopy, photo emission spectroscopy and X-ray diffraction. The corrosion behavior is evaluated by potentiodynamic polarization experiments and its dependence on the surface porosity is reported.

2. Experimental

Rectangular substrates 20×10×2 mm from commercial AISI H13 tool steel of composition 90.6 Fe, 0.5 C, 0.4 Mn, 1.0 Si, 5.1 Cr, 1.4 Mo, 0.9 V, (wt.%) were used for the experiments. The ferritic steel was pretreated by quenching and tempering (~590 °C) obtaining a martensitic microstructure. Before nitrocarburizing, the samples were mirror polished with diamond abrasive powder (1 μm), and ultrasonically cleaned in alcohol. The nitrocarburizing processes were performed in a commercial hot-wall, fully automatic Plasmatec180 pulsed plasma system, 60A/1000V (Plasma-LIITS, 13083-970 Campinas, São Paulo, Brazil) [20]. A low-pressure sputtering pre-cleaning was carried out with Ar and H_2 plasma during the heating of the samples up to the nitrocarburizing temperature (563 °C±5). The plasma nitrocarburizing process was performed at a constant pressure

* Corresponding author. Tel.: +55 19 3521 5377; fax: +55 19 3521 5376.
E-mail address: basso@ifi.unicamp.br (R.L.O. Basso).

0257-8972/$ – see front matter © 2008 Elsevier B.V. All rights reserved.
doi:10.1016/j.surfcoat.2008.10.006

of 400 Pa and at different treatment times (2, 5, 7, 10, 15 and 20 h). For the study, a gaseous mixture consisting of N_2 (87.3%), H_2 (9.7%), and CH_4 (3%) was used. The total flux was maintained constant at 0.35 slm. After the treatment, the samples were cooled down slowly (~6 h) inside the vacuum chamber. The treated samples were sliced and mounted in conductive Bakelite (Bakelite+powdered cupper) and mirror polished (0.05 μm) with colloidal silica suspension. The nitrocarburized layers were revealed, at room temperature, by etching the samples with Nital 2% (2% v/v nitric acid in absolute ethanol). The cross-section morphology and the thickness of the nitrocarburized layers were analyzed by SEM (JEOL JMS-5900LV). In order to quantify the nitrided material surface porosity, the samples were examined by image analysis using the software *Olympus analiSYS FIVE®* [21]. Ten different images of the nitrided samples were analyzed to calculate the porosity surface density. The phase composition of the compound layers were studied by X-ray diffraction analysis (XRD). The X-ray data were collected at room temperature between 20° and 100° (2θ) using a Philips diffractometer (PW1710) with Cu target and a graphite monochromator, scanning steps of 0.02° and 5 s counting step time at glancing incidence of 5°. The relative concentrations of main elements on the surface were obtained by X-ray photoelectron spectroscopy (XPS) using the 1486.6 eV (Kα-line) photons from an Al target and a VG-CLAM2 hemispherical analyzer. The total apparatus resolution was ~0.85 eV (line-width plus analyzer). The system details are reported elsewhere [22]. The relative atomic composition at the sample surfaces was determined by integrating the core level peaks, properly weighted by the photo-emission cross-section. As is well known, XPS gives information of the outmost atomic material layers (~0.5 nm) [23]. For the corrosion tests, the nitrocarburized area to be studied was defined by partially covering the sample with insulating resin. In this fashion, a 6×3 mm^2 area of the sample was exposed to the electrolyte solution. The reference electrode was a saturated calomel electrode (SCE). A platinum wire was used as counter electrode. The electrolyte was an aqueous solution containing 0.9 wt/V % NaCl. The oxygen dissolved in the solution was removed by bubbling dry N_2 with 1.5 L/min for 15 min, and afterwards for 45 min with 0.5 L/min. To keep the solution O_2 free during the corrosion tests, N_2 was gently fed into the cell, avoiding bubbling (0.5 L/min). For all electrochemical tests, a multi-potentiostat system VMP from Bio-logic S.A. was used. Potentiodynamic polarization tests were performed at 23 °C, 30 mV/min ramp, after 30 min recording the open circuit potential. The corrosion potential was determined from the I vs. E polarization curves by taking the value at the zero current point. This value is similar to that obtained by the intersection of Tafel lines [24]. The corrosion current (i_{corr}) was determined by employing the Stern–Geary equation given by [25]:

$$i_{corr} = \left[\frac{b_a b_c}{2.303(b_a + b_c)}\right]\left[\frac{1}{R_p}\right] \quad (1)$$

where R_p is the polarization resistance, defined by $R_p=(\Delta E/\Delta i)$ for $\Delta E \to 0$. Here, ΔE and Δi are the potential and current polarization variation, respectively. Therefore, the polarization resistance is obtained from the derivative of the i vs. E plots. The b_c and b_a values are the Tafel cathodic and anodic slope, respectively, obtained from the potentiodynamic polarization curves.

3. Results

3.1. Microstructure of the nitrocarburized layer

Fig. 1 displays the XRD patterns for the samples treated by plasma nitrocarburizing at several treatment times. From the diffraction patterns, four different phases can be identified in the nitrocarburized layer: α-martensitic steel phase (corresponding to the steel matrix), the ε-Fe_{2-3}(C,N) phase, the γ′-Fe_4N phase, and the CrN phase. On

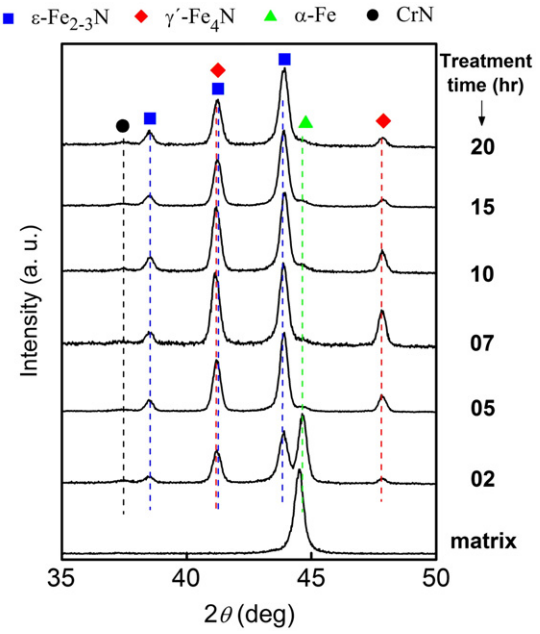

Fig. 1. Evolution of the XRD patterns as a function of treatment time. The different phases present in the material are indicated.

increasing treatment time, the α-martensite phase vanishes in thicker nitrocarburized layers, i.e., its contribution becomes less intense to the point of disappearing. In addition, the ε and γ' phases become dominant while γ′-Fe_4N peaks decrease for longer treatment times. Finally, we note that the CrN phase weakly appears after 7 h treatment.

The comparison of these results with the micrographs obtained from SEM is adding interesting information. Fig. 2 displays the scanning electron microscopy cross-section images of nitrocarburized samples during (a) 2, (b) 5, (c) 7, (d) 10 and (e) 20 h. In all the samples a compound layer is observed (outermost layer), followed by a diffusion layer. As revealed by XRD results, the compound layer is mostly constituted by the ε-Fe_{2-3}(C,N) and γ′-Fe_4N phases (Fig. 1). For lower treatment times, a thin (~1 μm) compound layer is obtained (Fig. 2a). At intermediate treatment times, the compound layer becomes thicker (~3 μm) and more homogeneous than at lower treatment times (Fig. 2c). At higher treatment times, despite achieving thicker compound layers, they become non-homogeneous and porous (see Fig. 2d and e). For example, after a 20 h process, the compound layer shows higher porosity on the nitrided surface. Fig. 3 shows the atomic content of the main elements in the nitrocarburized layer (Fe, C, N, Cr). Other constituent elements such as V, Mo, Si, and Mn do not change appreciably and will not be considered. As can be seen, the concentrations of Fe, N, and Cr reach a saturation level at 5 h of treatment. On the other hand, C concentration stays constant at all times, indicating that a surface de-carburization was prevented in the experimental conditions used in the experiments.

Although XPS provide the chemical information up to 5 nm of depth from surface, some behaviors of the nitrocarburized layer can be deduced because the methane partial pressure in the chambers was fixed, and only the treatment time was changed. The carbon chemical potential on the surface is constant and proportional to the carbon content in the nitrocarburized layer. The treated surface composition remains constant for treatment times longer than 5 h of plasma nitrocarburizing.

3.2. Corrosion tests

Fig. 4 displays the potentiodynamic polarization curves of the studied samples. The curve corresponding to the untreated substrate indicates that the H13 steel is relatively easily corroded in a NaCl

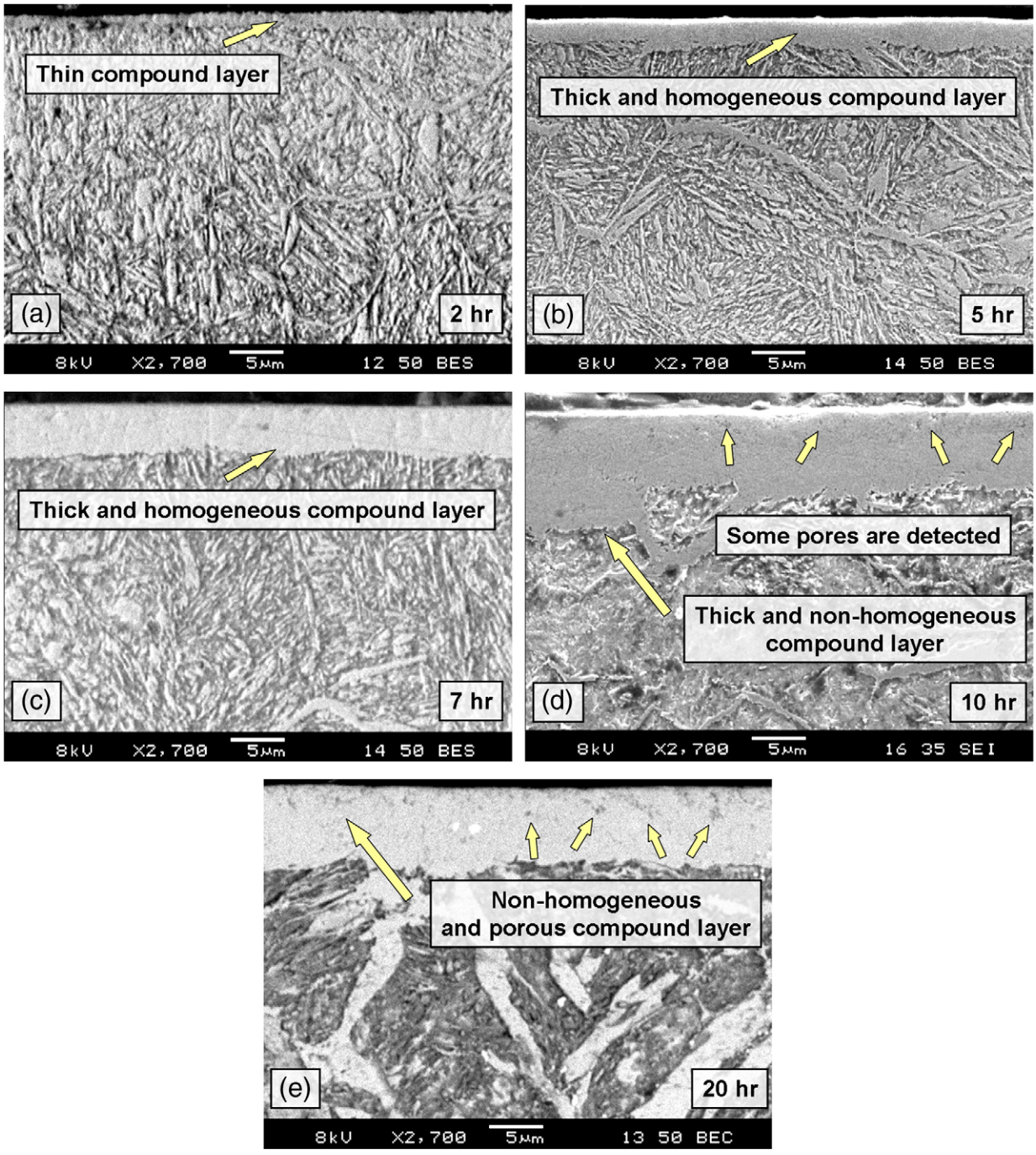

Fig. 2. Cross section microstructure obtained by SEM from samples plasma-nitrocarburized during 2h (a), 5h (b), 7h (c), 10h (d), and 20h (e). The phase mixture is clearly seen in the pictures.

solution. On the other hand, in the nitrocarburizing samples, the corrosion current at relatively high potentials (above −0.7 V) is relatively lower. As observed in the figure, the nitriding time profoundly influences the corrosion resistance of the material. For the shorter nitriding treatment times (2 h), the surface becomes passivated at −0.55 V (SCE). At −0.12 V, the nitrided protecting layer broke up, increasing the corrosion current, and an important pitting process takes place. As observed in the Fig. 4, for the intermediate treatment times (5 and 7 h), the best corrosion resistant behavior is obtained, as suggested, from the lower measured corrosion current. Finally, for longer nitriding treatment times (10 and 20 h), no increasing corrosion resistance is apparent. Indeed, Fig. 4 shows that the corrosion current notably increases in these samples. This is probably due to the fact that the nitrocarburized layer is porous and inhomogeneous (see Fig. 2d and e).

4. Discussion

Table 1 summarizes the most important parameters of the corrosion tests, obtained from the Stern–Geary equation (see Eq. (1)). Table 1 also included the porosity fraction of the nitrocarburized layer. As remarked in Section 2, the percentage of porous is obtained by image analysis of the SEM micrograph of the nitrocarburized samples. Fig. 5 shows a typical SEM micrograph of treated sample by 2 h. The presence of porous at the surface is clearly observed in the picture.

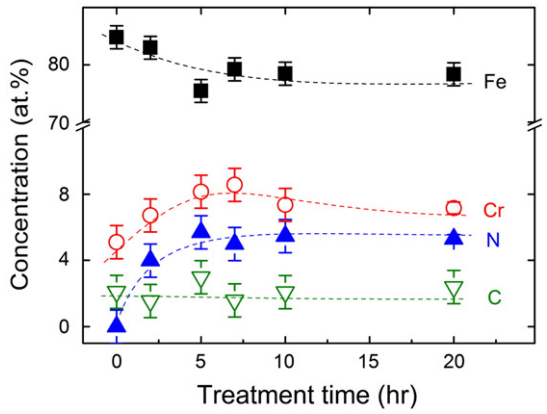

Fig. 3. The relative atomic percents of the most important elements on sample surface. The dash lines are a guide for the eyes.

The potentiodynamic polarization currents obtained at different constant potentials are analyzed as a function of the nitrocarburizing time process (Fig. 6B). One of the selected potentials is −0.6 V, i.e., the passivation potential from the curves corresponding to samples treated at 2, 10 and 20 h, respectively. The other selected potential (−0.3 V) is the so called *trans-passivation potential* for all the samples. This last potential is defined as the potential where an alteration in the behavior of the curves occurs, i.e., a turning point where a corrosion current increasing takes place. The result at 0 V applied potential is also displayed for comparison purposes with those studies at higher applied potentials. Moreover, the pristine material shows the highest corrosion at 0 V and −0.3 V corrosion potential (Fig. 6b, upside down triangles). A surprising results, however is observed in the pristine sample at −0.6 V corrosion potential (circled square symbol, Fig. 6b). This can be explained by the missing porosity in the mirror polished bare steel. The electrochemical behavior of the 2 h treated sample is somewhat similar to a corrosion resistant but porous layer overlying an active corroding substrate. The porous are pathways of connection between the environment and the substrate through the corrosion resistant nitrocarburized layer. Taking into account these facts, a decrease in porosity is mandatory in order to augment the corrosion resistance of surface treated steels [26].

For other potential range, however, even a short nitriding process of 2 h improves the material corrosion resistance. Although not completely passivated, the formation of a thin compound layer prevents strong corrosion of the bulk material. For intermediate treatment times (~5 h) the current is notably lower than before due to the formation of a thicker, homogenous compound layer granting good corrosion resistance (Fig. 2b and c).

Table 1
Corrosion parameters obtained by the Stern–Geary equation and porosity measurements

Treatment time (h)	E_{corr} (V) vs. (SCE)	R_p (Ω cm^2)	Porosity (%)	I_{corr} (A cm^{-2})×10^{-6}	b_a (V/dec)[a]	b_c (V/dec)[a]
0	−0.724	3795	–	7.0	0.111	0.137
2	−0.707	4433	29.79	4.5	0.051	0.413
5	−0.702	15,528	11.43	1.1	0.047	0.286
7	−0.705	5462	16.58	6.5	0.133	0.220
10	−0.725	2654	15.58	8.4	0.061	0.303
20	−0.714	2342	29.27	~10	0.076	0.354

[a] V/dec: volt by decade of change in current.

For the studied samples, the XRD patterns indicate that the compound layer is rich in the ε-Fe_{2-3}(C,N) and γ′-Fe_4N phases (Fig. 1). Above 7 h nitrocarburizing treatment times the corrosion current increases. Therefore, a too thick, non-homogeneous, and porous compound layer jeopardizes the corrosion resistance (Fig. 2d and e). This result is consistent with the observed CrN precipitation on longer treatment times. Indeed, the presence of a porous microstructure and CrN precipitation increases the pathways for pitting corrosion, augmenting the tendency to galvanic corrosion [27].

Li and Bell [9] have shown that the corrosion mechanism in martensitic stainless steel (MSS) and austenitic stainless steel (ASS), after plasma nitriding, is not the same. In ASS, the CrN precipitation is the main factor for the degradation of corrosion resistance compared to the untreated material. However, in MSS, the plasma nitriding treatment improves the corrosion resistance, even after CrN precipitation, compared to the untreated material. In our case, ε-Fe_{2-3}(C,N) and γ′-Fe_4N phases are, approximately, in the same proportion (in the nitrocarburized layer) after 5 h of plasma treatment and the quantity of CrN precipitation is low. So, the most important parameter for controlling the corrosion resistance of the nitrocarburized material is the change of thickness and porous microstructure of the nitrocarburized layer (see Table 1). Last but not least, the above results clearly show that the presence of the ε-Fe_{2-3}(C,N) and γ′-Fe_4N phases in the nitrocarburized layer does not guarantee the material inertness. The X-ray diffraction analysis (Fig. 1) shows a homogeneous structure. On the other hand, the XPS results show that the chemical composition of the nitrocarburized layer of the studied samples essentially does not change on increasing treatments times (Fig. 3). This observation suggests that beyond 5 h treatment absence of porosity is the main cause preventing corrosion. Indeed, Ahn et al. [27] studied the room temperature corrosion behavior of CrN coated H13 tool steel in a 3.5%

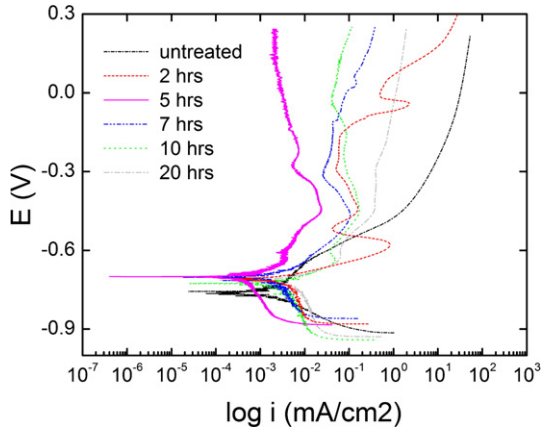

Fig. 4. Dynamic polarization curves obtained from some of the studied samples. The nitrocarburizing process time used in each sample is indicated.

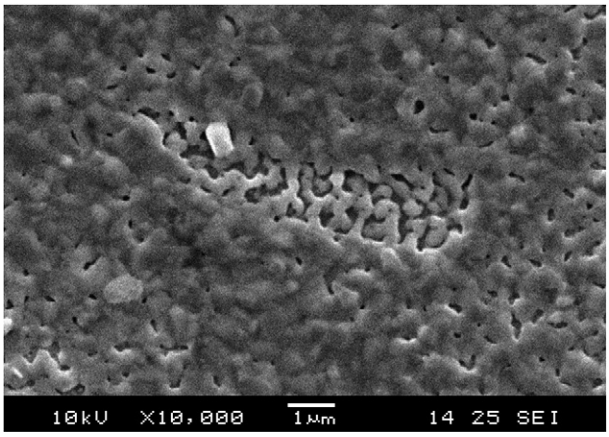

Fig. 5. SEM micrograph of top surface microstructure from the 2h plasma nitrocarburized sample.

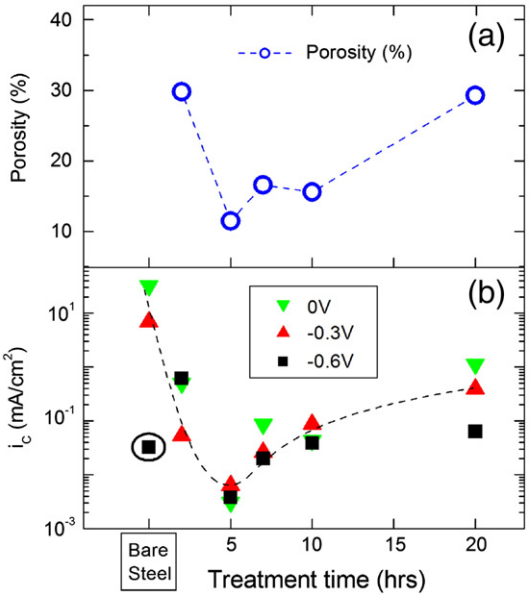

Fig. 6. (a) Measured porosity by image analysis of the SEM micrographs on surface samples; (b) current density measured at different applied potentials (0V, −0.3V and −0.6V) (SCE) for nitrocarburized samples and the bare steel. The circled square symbol indicates the different behavior of bare steel on the range of −0.6V (SCE). The dashed lines are guides for the eyes.

NaCl solution concluding that the corrosion is also associated with the film porosity. Also, Yoo et al. [28] pointed out that improved corrosion resistance are associated with lowest porosity in hard coated H13 steel.

5. Conclusions

The influence of the nitrocarburizing obtained by pulsed DC plasma on the corrosion behavior of AISI H13 tool steel was studied. The corrosion performance of the treated samples was evaluated by potentiodynamic polarization experiments. The importance of the microstructure of the nitrocarburized layers was established by a comprehensive study involving scanning electron microscopy, photoemission spectroscopy, and X-ray diffraction techniques. Appropriated nitrocarburized layers improve the material corrosion resistance. The treatment conditions determining thickness, porosity, composition, and microstructure are fundamental to control the corrosion resistance of the material. For short treatment times (<2 h) the formed thin (1–5 μm) compound layer shows relatively poor corrosion resistance. At intermediate treatment times (5 and 7 h) a thicker (~5–10 μm), homogeneous compound layer is formed, guaranteeing good corrosion resistance of the material. Finally, for longer treatment times (>7 h) an inhomogeneous, porous and thicker (>10 μm) compound layer is obtained displaying poor corrosion resistance. The presence of the ε-Fe_{2-3}(C,N) and γ′-Fe_4N phases in the nitrocarburized layer does not guarantee the material inertness and the control of porosity in mandatory in order to sustain the corrosion resistance. Therefore, a nitrocarburized layer must be thick, homogenous and free of porous and cracks to achieve a high corrosion resistance.

Acknowledgments

The authors are indebted to the *Laboratório de Implantação Iônica e Tratamento de Superfícies* (LIITS) and the *Laboratório Nacional de Luz Sincrotron* (LNLS). This work is part of the Ph.D. requirements of RLOB and was partially supported by FAPESP (grant # 05/53926-1). FA and RLOB are Fapesp and CNPq fellows, respectively. RJC is a member of CONICET and CAPES-SPU supported his sojourn at the IFGW. At the present, CAF is at the CCET, *UCS, CEP 95070-560, Caxias do Sul, Rio Grande do Sul, Brazil.*

References

[1] T.H. Zhang, C.Z. Ji, J.D. Xie, J. Chen, F.H. Wei, G.R. Sun, Y.Z. Gao, Vacuum 45 (1994) 945.
[2] T.M. Wang, J. Shi, X.S. Zhang, Nucl. Instrum. Methods. B 72 (1992) 55.
[3] S. Picard, J.B. Memet, R. Sabot, J.L. Grosseau-Poussard, J.P. Rivière, R. Meilland, Mater. Sci. Eng. A 303 (2001) 163.
[4] W. Liang, Appl. Surf. Sci. 211 (2003) 308.
[5] D. Wang, S. Ziyuan, Z. Longjiang, Appl. Surf. Sci. 214 (2003) 304.
[6] A. Persson, J. Bergström, C. Burman, S. Hogmark, Surf. Coat. Technol. 146 (2001) 42.
[7] A. Fossati, F. Borgioli, E. Galvanetto, T. Bacci, Surf. Coat. Technol. 200 (2006) 3511.
[8] C.L. Liu, P.K. Chu, G.Q. Lin, M. Qi, Surf. Coat. Technol 201 (2006) 2802.
[9] C.X. Li, T. Bell, Corrosion Science 48 (2006) 2036.
[10] J. Flis, M. Kuczynska, J. Electrochem. Soc. 151 (2004) B573.
[11] M.U. Devi, O.N. Mohanty, Surf. Coat. Technol. 107 (1998) 55.
[12] T. Bell, Y. Sun, A. Suhadi, Vacuum 59 (2000) 14.
[13] T. Liapina, A. Leineweber, E.J. Mittemeijer, W. Kockelmann, Acta Materialia 52 (2004) 173.
[14] F. Tessier, A. Navrotsky, R. Niewa, A. Leineweber, H. Jacobs, S. Kikkawa, M. Takahashi, F. Kanamaru, F.J. DiSalvo, Solid State Sciences 2 (2000) 457.
[15] J.M.D. Coey, P.A.I. Smith, J. Magn. Magn. Mater. 200 (1999) 405.
[16] T. Bell, Heat Treat. Met. 2 (1975) 39.
[17] A. Wells, J. Mater. Sci. 20 (1985) 2439.
[18] R.L.O. Basso, C.A. Figueroa, L.F. Zagonel, H.O. Pastore, D. Wisnivesky, F. Alvarez, Plasma Process Polymers 4S1 (2007) S728.
[19] A. Suhadi, C.X. Li, T. Bell, Surf. Coat. Technol. 200 (2006) 4397.
[20] L.F. Zagonel, C.A. Figueroa, R. Droppa-Jr, F. Alvarez, Surf. Coat. Technol. 201 (2006) 452.
[21] http://www.olympus.co.jp/en/insg/ind-micro/product/analysisfive/.
[22] P. Hammer, N.M. Victoria, F. Alvarez, J. Vac. Sci. Technol. A 16 (1998) 2941.
[23] D. Briggs, M.P. Seah, Practical Surface Analysis, Auger and X-ray Photoelectron Spectroscopy, John Wiley & Sons, New York, 1990.
[24] V.K.W. Grips, V.E. Selvi, H.C. Barshilia, K.S. Rajam, Electrochimica Acta 51 (2006) 3461.
[25] W.H. Ailor, Hadbook of Corrosion Testing and Evaluation, Jhon Willey, New York, 1971, p. 184.
[26] J. Creus, H. Idrissi, H. Mazille, F. Sanchette, P. Jacquot, Surf. Coat. Technol. 107 (1998) 183.
[27] S.H. Ahn, Y.S. Choi, J.G. Kim, J.G. Han, Surf. Coat. Technol. 150 (2002) 319.
[28] Y.H. Yoo, D.P. Le, J.G. Kim, S.K. Kim, P.V. Vinh, Thin Solid Films 516 (2008) 3544.